Biochemistry

 Volume 34, Number 21 May 30, 1995

Accelerated Publications

Solution Structure of the Ras-Binding Domain of c-Raf-1 and Identification of Its Ras Interaction Surface‡

S. Donald Emerson, Vincent S. Madison, Robert E. Palermo, David S. Waugh, Julie E. Scheffler, Kwei-Lan Tsao, Susan E. Kiefer, Shuang P. Liu, and David C. Fry*

Roche Research Center, Hoffmann-La Roche Inc., Nutley, New Jersey 07110

Received March 1, 1995; Revised Manuscript Received April 17, 1995⊗

ABSTRACT: The structure of the Ras-binding domain of human c-Raf-1 (residues 55−132) has been determined in solution by nuclear magnetic resonance (NMR) spectroscopy. Following complete assignment of the backbone and side-chain ^{1}H, ^{15}N, and ^{13}C resonances, the structure was calculated using the program CHARMM. Over 1300 NOE-derived constraints were applied, resulting in a detailed structure. The fold of Raf_{55-132} consists of a five-stranded β-sheet, a 12-residue α-helix, and an additional one-turn helix. It is similar to those of ubiquitin and the IgG-binding domain of protein G, although the three proteins share very little sequence identity. The surface of Raf_{55-132} that interacts with Ras has been identified by monitoring perturbation of line widths and chemical shifts of ^{15}N-labeled Raf_{55-132} resonances during titration with unlabeled Ras−GMPPNP. The Ras-binding site is contained within a spatially contiguous patch comprised of the N-terminal β-hairpin and the C-terminal end of the α-helix.

Raf-1 is an immediate downstream target of Ras[1] in a signal transduction pathway that controls cell growth and differentiation (Moodie et al., 1993; Van Aelst et al., 1993; Vojtek et al., 1993; Warne et al., 1993; Zhang et al., 1993). Prolonged signaling by mutant forms of Ras is associated with cellular transformation and numerous human cancers (Barbacid, 1987). Since oncogenic Ras variants retain their ability to bind to Raf (Zhang et al., 1993; Chuang et al., 1994; Herrmann et al., 1995), compounds that disrupt the Ras−Raf interaction may have therapeutic benefits. While high-resolution structures of Ras have been obtained from X-ray and NMR studies (deVos et al., 1988; Brunger et al., 1990; Pai et al., 1990; Tong et al., 1991; Kraulis et al., 1994), information about the structure of Raf will also be valuable for the design of inhibitors. In addition, since Ras has been shown to interact with several other proteins, such as GAP, neurofibromin, guanine nucleotide exchange factors (GEFs), and 3-hydroxyphosphatidylinositol kinase [PI(3)K] (Trahey & McCormick, 1987; Vojtek et al., 1993; Rodriguez-Viciana et al., 1994), details of the Ras−Raf interaction may provide insights on general strategies by which Ras complexes with its protein targets.

Raf is a 72 kDa serine−threonine protein kinase that possesses a catalytic domain and two other conserved regions (Heidecker et al., 1992). One conserved region includes the Ras-binding domain, which has been mapped to residues 55−132 (Vojtek et al., 1993; Scheffler et al., 1994). Preliminary NMR characterization of Raf_{55-132} has revealed that it is a highly ordered protein domain (Emerson et al., 1994). We now report a detailed solution structure for Raf_{55-132} as

‡ Coordinates have been deposited in the Brookhaven Protein Data Bank (file name 1RFA).

⊗ Abstract published in *Advance ACS Abstracts,* May 15, 1995.

[1] Abbreviations: Raf_{55-132}, a polypeptide consisting of residues 55−132 of human c-Raf-1 with an additional alanine residue at the N-terminus; Ras, the 21 kDa protein product of the ras oncogene; NMR, nuclear magnetic resonance; NOE, nuclear Overhauser effect; NOESY, nuclear Overhauser effect spectroscopy; TOCSY, total correlation spectroscopy; HSQC heteronuclear single-quantum correlation; HMQC, heteronuclear multiple-quantum correlation; GMPPNP, β,γ-imidoguanosine 5′-triphosphate; rmsd, root mean square deviation.

0006-2960/95/0434-6911$09.00/0

determined by NMR spectroscopy. Further, the localized region that interacts with Ras is identified from resonance perturbation mapping experiments. These NMR results are used to propose specific interactions between Raf and Ras which are consistent with available mutagenesis data.

MATERIALS AND METHODS

Sample Preparation. The expression and purification of Raf_{55-132} have been described in detail (Scheffler et al., 1994; Emerson et al., 1994). NMR samples contained 1.4 mM uniformly ^{15}N- or $^{13}C/^{15}N$-labeled Raf_{55-132} in 10 mM sodium acetate-d_3, pH 5.3, 0.1 mM dithiothreitol, and 0.05% sodium azide in 100% D_2O or 94% H_2O/6% D_2O.

NMR Spectroscopy. NMR experiments were run at 25 °C on a Varian UNITY*plus*-600 spectrometer. Data were processed using FELIX software (BioSym). The assignment of backbone ^1H, ^{13}C, and ^{15}N resonances was accomplished as described previously (Emerson et al., 1994). Through-bond correlations of side-chain resonances were made from analysis of 3D $^1H-^1H-^{15}N$ TOCSY-gradient HSQC (H_2O sample) and 3D HCCH-TOCSY (D_2O sample) experiments (Bax et al., 1990). NOEs were obtained from 3D $^1H-^1H-^{15}N$ NOESY-gradient HSQC (H_2O sample) and 3D $^1H-^1H-^{13}C$ NOESY-HMQC (D_2O sample) experiments (Ikura et al., 1990). NOESY mixing times were 125 ms. Water suppression and heteronuclear coherence selection for F_2F_3 $^1H-^{15}N$ planes of the 3D $^1H-^1H-^{15}N$ NOESY-gradient HSQC and $^1H-^1H-^{15}N$ TOCSY-gradient HSQC were accomplished using phase-sensitive, pulsed field gradients (Davis et al., 1992). Soft preirradiation ($\gamma H_2 = 20$ Hz for 1.2 s) was utilized to suppress exchange peaks from H_2O. Pure phase F_1F_3 $^1H-^1H$ planes were collected using the hypercomplex strategy with F_1-axial displacement (Marion et al., 1989). NH exchange rates were measured by acquiring sensitivity-enhanced, phase-sensitive, gradient-selected $^1H-^{15}N$ HSQC(Kay et al., 1992) spectra vs time after dissolution of lyophilized ^{15}N-Raf_{55-132} into D_2O.

Structure Calculation. Our procedure for calculating structures was that previously described (Fry et al., 1992), with the following modifications. An updated version (version 22) of the CHARMM program and parameter set (Brooks et al., 1983) was used. A total of 1303 NOEs were utilized in the calculations, of which 299 were long range ($|i - j| \geq 5$). NOEs were converted into distance constraints (r_0) using the approaches for volume measurement, calibration, and uncertainty assessments described by Wagner and co-workers (Hyberts et al., 1992). This approach involves cross-peak integration using FELIX software and distance calibration by a collective consideration of NOEs involving protons whose distance apart is fixed within a narrow range. In order to apply our distance constraints in a conservative manner, to allow for uncertainties in NOE measurements and the assumptions inherent in the distance calibrations, we added larger uncertainty ranges to the distances by modifying the error function equations to the following forms: $r_{lower} = 1/(1.4/r_0^6 + 1/5.84^6)^{1/6} - 0.50$; $r_{upper} = 1/(0.7/r_0^6 - 1/5.84^6)^{1/6} + 0.50$. These equations resulted in uncertainty ranges about the distances of at least ±20%. Each 20 ps cycle of high-temperature dynamics used successive pairs of 0.3, 2; 3.0, 2; 0.6, 4; 3.0, 4; 0.5, 8; and 0.05, 12 for WNOE and ENOE, where WNOE is the weighting factor for the NOE constraint energy and ENOE is the exponent. Quenching and minimization used only the last pair of values. The floating chirality algorithm was extended to include both partners for NOEs involving two chiral protons. This algorithm (Fry et al., 1992) is applied at each iteration step and chooses the stereospecific assignment which gives the best fit to all of the distance constraints for prochiral methyl and methylene groups that exhibit separate chemical shifts. Thirty structures were calculated. The 1303 NOE-derived constraints applied were well satisfied, with only one exhibiting an average rmsd that was more than 0.5 Å beyond the error limits. Rmsd values concerning the similarity and precision of the structures are given in the Results section.

Mapping of the Ras Interaction Surface. The initial sample for the Ras titration experiment consisted of 0.77 mM ^{15}N-Raf_{55-132}, 10 mM sodium acetate-d_3, pH 5.3, 0.1 mM dithiothreitol, 5 mM $MgCl_2$, and 0.05% NaN_3 in 94% H_2O/6% D_2O. A stock solution of Ras was prepared that consisted of 2.3 mM full-length N-Ras(Asp^{12})−GMPPNP, 10 mM sodium acetate-d_3, pH 5.3, 0.1 mM dithiothreitol, 5 mM $MgCl_2$, and 0.05% NaN_3 in 94% H_2O/6% D_2O. Ras was expressed and purified as described previously (Trahey et al., 1987), and the methods used for preparing the GMPPNP-bound form have been reported (John et al., 1990). Two-dimensional $^1H-^{15}N$ HSQC experiments were performed using pulsed field gradients to select the desired heteronuclear coherence pathway and to suppress the water resonance (Kay et al., 1992). Cross-peak intensities were measured using VNMR software. An HSQC spectrum was acquired on the initial Raf sample. Additions of the Ras stock solution were made in a stepwise manner to the Raf sample. At each step, an HSQC spectrum was acquired. The total sample volume was allowed to increase, beginning at 380 μL in a 4-mm tube and ending at 725 μL in a 5-mm tube. Additions were made to a final Ras:Raf concentration ratio of 2.75:1. In the final sample, the concentrations of Ras and Raf were 1.1 mM and 0.4 mM, respectively.

RESULTS AND DISCUSSION

Tertiary Structure of Raf_{55-132}. Complete assignments were made for the backbone and side-chain ^1H, ^{15}N, and ^{13}C resonances of Raf_{55-132} from a series of three-dimensional heteronuclear NMR experiments acquired on ^{15}N- and $^{13}C/^{15}N$-labeled versions of the protein. The structure was determined by applying 1303 NOE-derived interproton distances as constraints in molecular dynamics calculations, using the program CHARMM. Stereospecific assignments of prochiral resonances were made by a custom algorithm added to CHARMM that allowed for floating chirality at each center and selected the assignment which best satisfied all of the NOE constraints.

A set of 30 structures was obtained from the molecular dynamics calculations. The experimental constraints were well satisfied, with an average root mean square deviation (rmsd) from the target distances of 0.65 Å and an rmsd in excess of the error limits of 0.13 Å (Table 1). Thirty of the 44 β-methylene groups that exhibited separate chemical shifts were stereospecifically assigned by the floating chirality algorithm. Our criterion for stereo assignment required agreement among 26 or more of the 30 structures (that is, >87% agreement). Also, 9 of the 16 Leu $C\delta H_3$ and Val $C\gamma H_3$ pairs that exhibited separate chemical shifts were stereospecifically assigned. Comparison of the calculated

Table 1: Structure Calculation Statistics

NOE Constraints type	no. of constraints
total	1303
intraresidue	625
interresidue sequential ($\|i-j\|=1$)	276
interresidue short range ($1<\|i-j\|<5$)	103
interresidue long range ($\|i-j\|\geq 5$)	299

Final Structural Statistics	
constraint deviations[a]	
rmsd from the target distances	0.65 Å
rmsd in excess of error limits	0.13 Å
no. of violations >0.5 Å beyond error limits	1
precision of structures	
rmsd from the average: Cα backbone atoms	0.60 Å
rmsd from the average: all atoms	1.1 Å

[a] Values are averages for the 30 calculated structures.

structures indicates that the conformation of Raf_{55-132} is well determined (Figure 1a,b), with an rmsd from the average of only 0.60 Å for the Cα backbone atoms and 1.1 Å for all heavy atoms (Table 1). A more detailed assessment of the local variability of backbone Cα positions is provided by a plot of rmsd vs residue number (Figure 2). Figure 2 illustrates that the best determined regions of the protein have Cα rmsd values on the order of 0.2−0.4 Å. Buried side chains were generally well determined, while exposed side chains, as expected, were less precisely defined (Figure 1b).

The structure of Raf_{55-132} consists of a five-stranded β-sheet, a 12-residue α-helix, and an additional one-turn helix (Figure 1c). The backbone topology begins with an antiparallel pair of β-strands (residues 57−62 and 67−72) arranged in a hairpin configuration. The conformation near Asn^{64}, in the turn between the two strands, is not well defined by the NOE constraints. This region appears to be highly solvent-accessible, as judged by the exchange rate of the Asn^{64} backbone NH proton, which is the most rapid of the backbone NH protons. After the second β-strand, there is a small connecting loop, consisting of residues 73−76, which is poorly defined by the NOE data. The α-helix is comprised of residues 78 through 89. Following the C-terminus of the helix, an extended, comparatively well-ordered linker segment runs from residues 90 to 95. The next β-strand (residues 96−100) is arranged in an antiparallel manner with the remaining two β-strands (residues 108−111 and 125−129) in a partial Greek-key motif. Between the third and fourth β-strands, residues 101−107 form a wide, isolated loop. These residues exhibit rapid NH exchange rates. Residues 113−117 are in an extended conformation. Residues 118−121 comprise a distorted, one-turn helix. The C-terminal β-strand (residues 125−129) forms a parallel pair with the N-terminal β-strand (residues 57−62) to complete the β-sheet. The terminal residues (55 and 132) appear to be highly mobile, as evidenced by the narrow line widths of their proton resonances.

The extended segment comprised of residues 113−117 acts as an antiparallel N-cap for the α-helix, with the carbonyl groups of Trp^{114} and Thr^{116} hydrogen bonded to the amide protons of His^{79} and Leu^{78}, respectively. This is an uncommon arrangement. In their initial description of N-capping, Presta and Rose (1988) noted that only 5% of the proteins they surveyed utilized a remote segment to supply hydrogen-bonding partners for an N-cap.

Raf_{55-132} possesses a hydrophobic core that is composed of the side chains of Phe^{99}, Trp^{114}, and most of the Ala, Val, Leu, and Ile residues. The α-helix contains three leucines spaced four residues apart (positions 78, 82, and 86) along one side, which project into the core and serve to pack the helix against the rest of the protein. There are two exposed aromatic groups, Phe^{61} and Phe^{130}. Most of the charged side chains are oriented toward the surface. An exception is the side chain of Lys^{109}, which is positioned along the face of Phe^{99} and appears to be held in place by an ionic interaction with Asp^{129}.

The topology of Raf_{55-132} is similar to those of ubiquitin and the IgG-binding domain of protein G, proteins of comparable size whose structures have been solved by X-ray and NMR methods (DiStefano & Wand, 1987; Vijay-Kumar et al., 1987; Weber et al., 1987; Gronenborn et al., 1991; Achari et al., 1992; Lian et al., 1992) (Figure 3). The spatial positioning of the first two N-terminal and the last C-terminal β-strands is nearly identical in the three proteins, and in all of them the α-helix is packed diagonally against part of the β-sheet. Overall, Raf_{55-132} resembles ubiquitin very closely except that one of the connecting loops is larger in Raf (residues 101−108). Protein G differs from the other two proteins in the angle between the helix and strand axes, in the deletion of a large loop, and in the manner in which the fourth strand is positioned in the β-sheet. A comparison of shared elements of secondary structure reveals that 48 Cα pairs from Raf and ubiquitin can be superimposed with an rmsd of 1.5 Å, and 25 Cα pairs from Raf and protein G can be superimposed with an rmsd of 1.7 Å. The structural similarity of the three proteins was unexpected since they share very little sequence identity (0−12%, depending on which pair is compared). However, sequence alignment of the proteins based on their three-dimensional structures reveals that conservation of the physical character of the residues (classified as hydrophobic, charged, or polar-neutral) is much higher (30−45%). There is no functional similarity among the three proteins, except that they all have been implicated in protein−protein interactions.

Ras−Raf Interactions. The interaction of Raf_{55-132} with Ras was studied by heteronuclear NMR. In order to selectively monitor Raf during formation of the complex, uniformly ^{15}N-labeled Raf_{55-132} was used in conjunction with unlabeled Ras. Ras switches between two specific conformations depending on whether GDP or GTP occupies the nucleotide-binding site (Pai et al., 1989; Milburn et al., 1990; Miller et al., 1992). Raf exhibits high-affinity binding to Ras−GTP (Moodie et al., 1993; Van Aelst et al., 1993; Vojtek et al., 1993; Warne et al., 1993; Zhang et al., 1993), although a K_D value has not been directly determined under the exact conditions of the NMR study. Ras bound with GMPPNP was prepared, in order to avoid complications from the inherent slow hydrolytic activity of Ras. N-$Ras(Asp^{12})$ was used because of its greater solubility and stability as a GTP complex. The binding interactions were monitored by acquiring two-dimensional $^1H-^{15}N$ HSQC spectra of Raf_{55-132}, first in the absence of Ras and then at each step of a systematic addition of Ras to the sample.

Each resonance of Raf_{55-132} responded in one of three ways to the addition of Ras: (1) no change or only a minor amount of broadening and chemical shift perturbation; (2) significant alteration of chemical shift for the ^1H and/or the ^{15}N resonance, accompanied by a diminution in intensity of

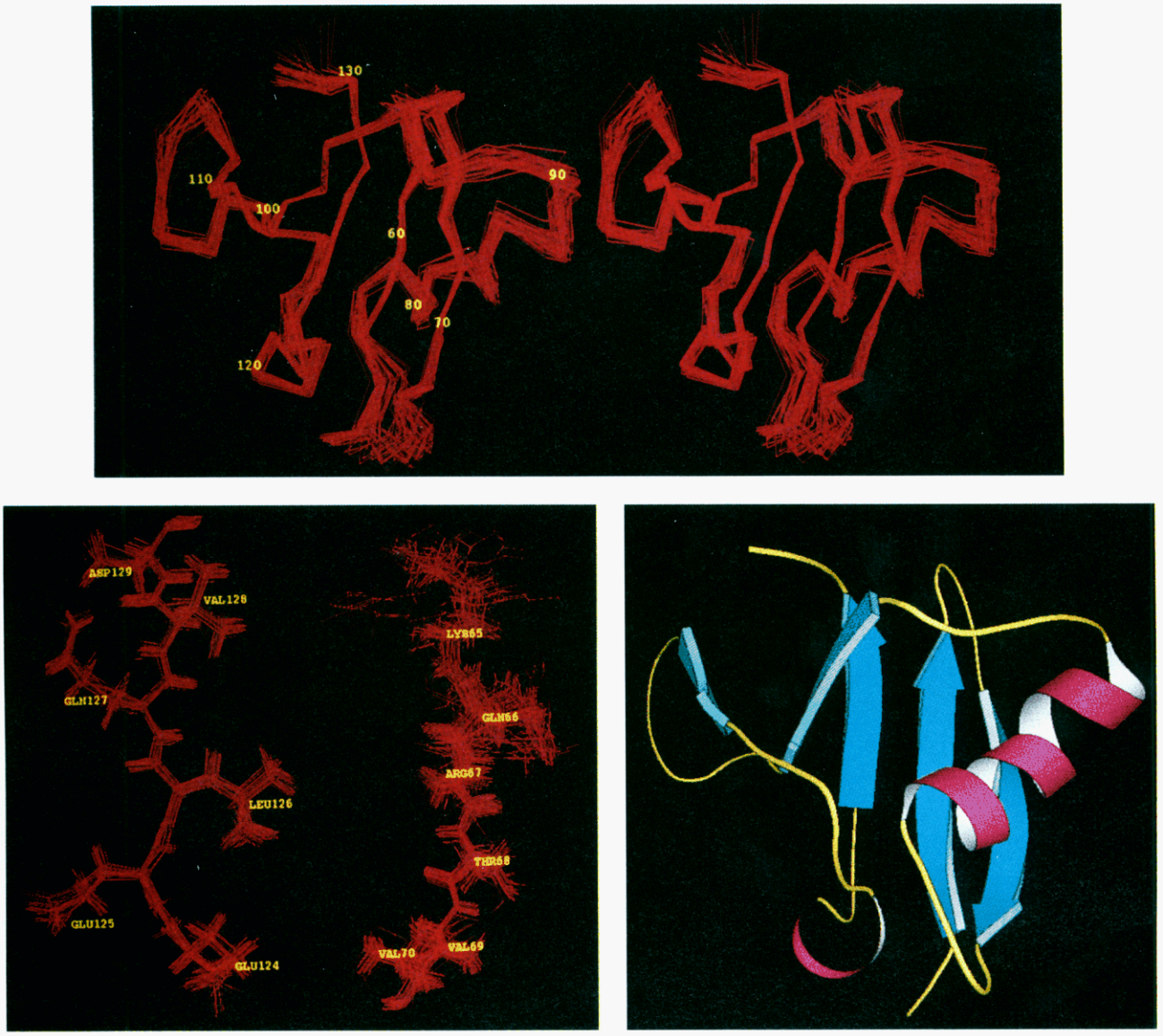

FIGURE 1: (a, top) Superposition of the 30 solution structures calculated for Raf_{55-132}, showing only the backbone atoms, in stereo. (b, bottom left) Superposition of thirty structures for selected regions of Raf_{55-132}, showing all atoms. Left: residues 124−129, representative of the precision with which nonexposed side chains were determined; right: residues 65−70, representative of exposed side chains. (c, bottom right) Simplified diagram of the tertiary fold of Raf_{55-132}. The lowest-energy structure from among the 30 calculated structures is depicted. The figure was created using the program MOLSCRIPT (Kraulis, 1991).

the HSQC cross-peak; or (3) "disappearance" of the HSQC cross-peak, presumably associated with large chemical shift changes. At saturating levels of Ras (>2:1 ratio), "new" unassigned cross-peaks were evident, which ostensibly represented those resonances which had undergone large chemical shift changes. Chemical shift alterations were not uniform and occurred in both upfield and downfield directions. Figure 4 shows one step in the titration (1:1 ratio), where the intensities for individual resonances in the absence (black) and presence (red) of Ras can be readily compared.

Signals which experienced small chemical shift changes (≤40 Hz) remained as single peaks with averaged chemical shifts throughout the titration (fast exchange behavior). Assuming a diffusion controlled on-rate (10^7-10^9 M^{-1} s^{-1}), this observation is consistent with a lower limit for K_D in the range of 40 nM to 4 μM under the conditions of the titration. Signals which were not observed as single averaged peaks throughout the titration presumably experienced chemical shift changes sufficiently large to allow exchange behavior in the intermediate to slow regime.

The region of Raf_{55-132} that interacts with Ras was identified by measuring the perturbations observed in the titration study and then mapping these results onto the structure. The resonances of Raf_{55-132} whose magnitudes were most dramatically reduced during the titration (boxed residues in Figure 4) were classified as "most perturbed" (colored magenta in Figure 5a,b). Almost all of the most perturbed residues are located in the N-terminal region of the protein; they are Asn^{56}, Ile^{58}, Arg^{59}, Val^{60}, Phe^{61}, Lys^{65}, Gln^{66}, Arg^{67}, Thr^{68}, Val^{69}, Leu^{78}, Met^{83}, Val^{88}, Arg^{89}, and Leu^{91}. In addition, there is one residue from the C-terminal half of the protein: Gln^{127}. It should be noted that Pro^{63} and Pro^{93} could not be monitored because they lack NH protons nor could Asn^{64} due to the rapid exchange of its NH proton.

Mapping the perturbation results onto the three-dimensional structure of Raf_{55-132} vividly reveals that the primary binding site is a localized patch on one side of the protein (Figure 5a). Fourteen of the 16 residues in the most perturbed class are gathered at the loop end of the β-hairpin

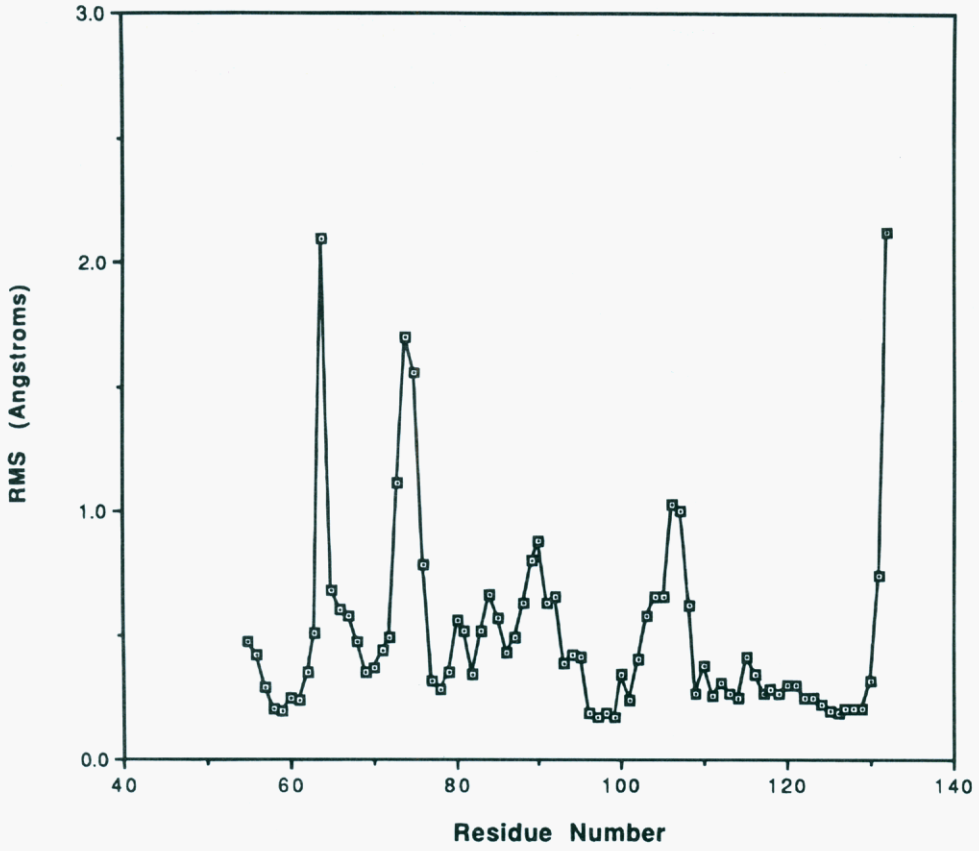

FIGURE 2: rmsd from the average structure, at each residue, for the Cα atoms of Raf_{55-132}.

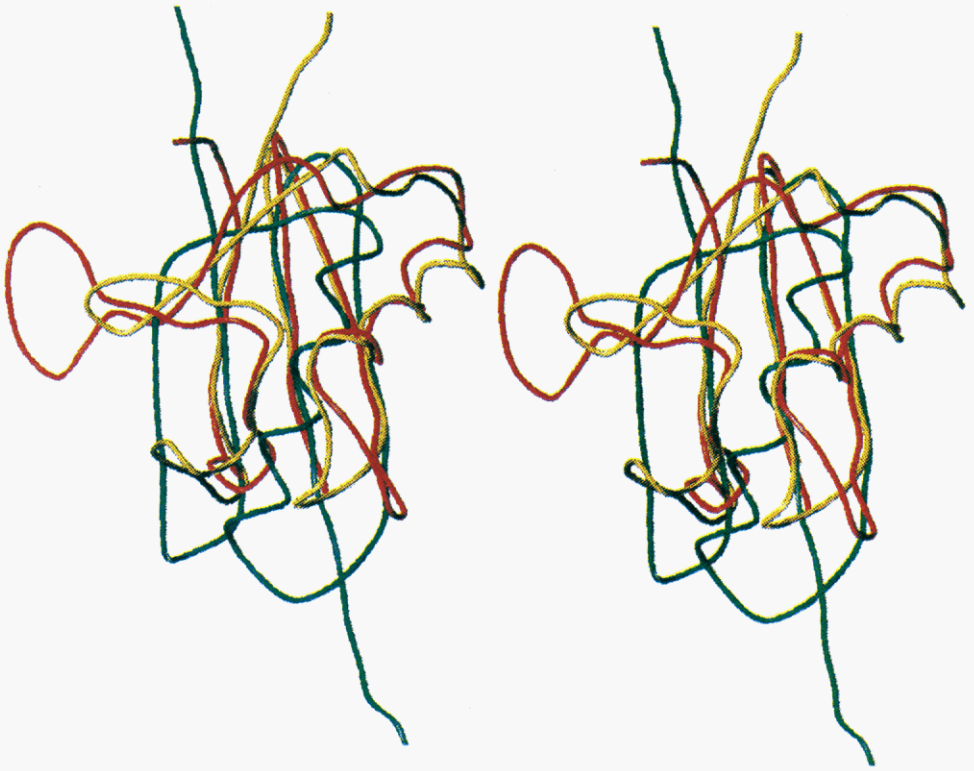

FIGURE 3: Stereo overlay of the backbone structures of Raf_{55-132} (red), ubiquitin (yellow) (Vijay-Kumar et al., 1987), and domain II of protein G (green) (Achari et al., 1992).

and at the C-terminal end of the α-helix (Figure 5b), suggesting that Ras makes its major contact with this region. These structural elements jut out from the body of the protein. The other two residues are remote from the primary contact site. Leu^{78} has a buried side chain and is located at the N-terminal end of the α-helix. Its perturbation is probably due to a minor reorientation of the helix which accompanies Ras binding. Asn^{56} is located near the base of the β-hairpin.

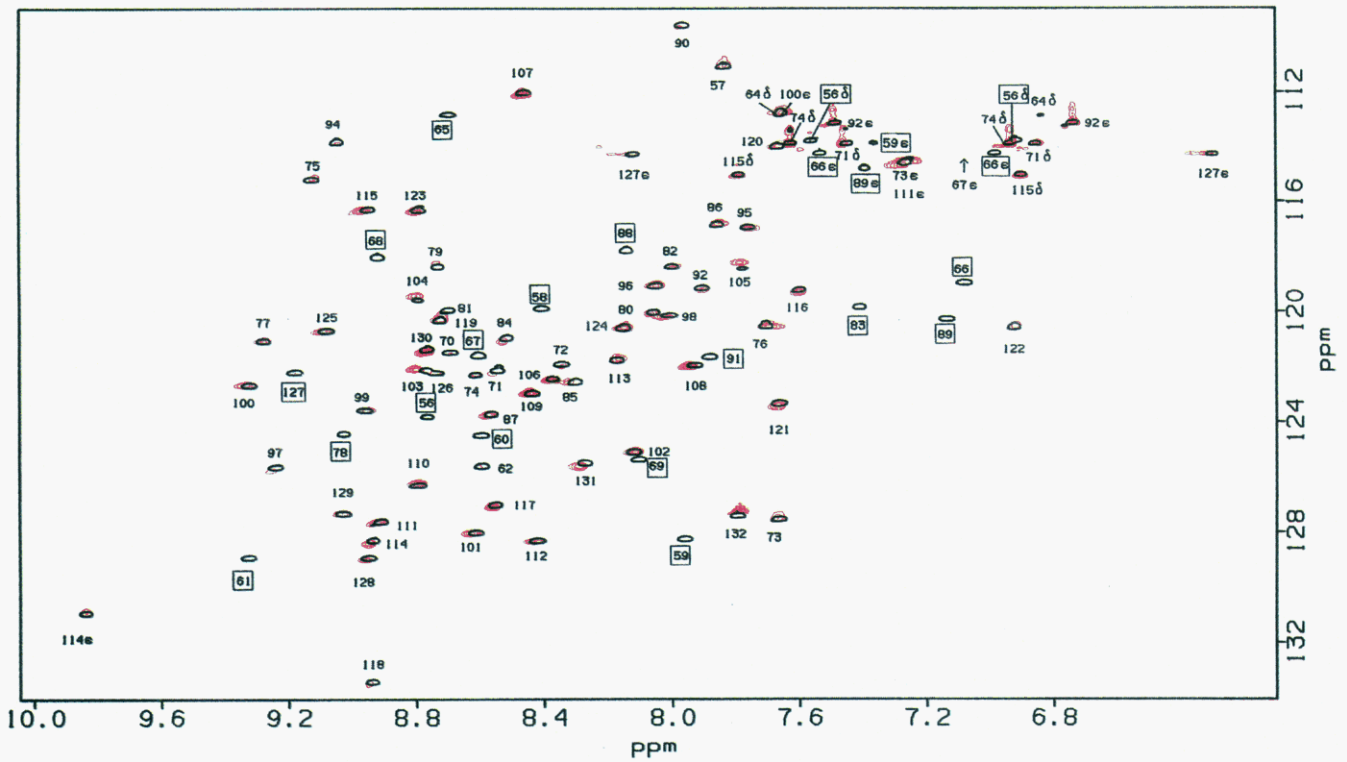

FIGURE 4: Superposition of 2D $^{1}H-^{15}N$ HSQC spectra of ^{15}N-labeled Raf_{55-132} alone (black) and in the presence of a 1:1 concentration ratio of unlabeled Ras−GMPPNP (red). Protein concentrations were 1.4 mM Raf_{55-132} (black) and 0.6 mM for both Raf_{55-132} and Ras−GMPPNP (red) in a buffer consisting of 10 mM sodium acetate-d_3, pH 5.3, 0.1 mM dithiothreitol, 5 mM $MgCl_2$, and 0.05% NaN_3 in 94% H_2O/6% D_2O. The spectra have been plotted at approximately equivalent signal-to-noise levels, with three contours shown for the black spectrum and complete contours shown for the red spectrum. Cross-peaks are labeled by residue number. The Greek letters indicate Trp NϵH, Asn NδH_2, Gln NϵH_2, and Arg NϵH (aliased) protons. An arrow indicates the position of the Arg 67 NϵH cross-peak, which is too small to be seen at this intensity level. Raf residues that were "most perturbed" (see text) by the addition of Ras−GMPPNP are boxed.

The effect seen there is probably also indirect.

All but three of the most perturbed residues have side chains that are solvent-exposed. Some of the exposed side chains contain nitrogen-attached protons and could be monitored in the HSQC spectra. Strong chemical shift and intensity perturbations were observed for the resonances of the side-chain NH_2 moieties of Asn^{56} and Gln^{66} and the NϵH moieties of Arg^{59} and Arg^{89}. This indicates that perturbed residues, defined on the basis of effects upon backbone NH resonances, could be making important side-chain interactions with Ras. The exposed side chains in the primary binding site include hydrophobic groups (Phe^{61}, Val^{69}, Val^{88}, and Leu^{91}) and basic groups (Arg^{59}, Lys^{65}, Arg^{67}, and Arg^{89}). No acidic side chains are involved.

Support for the functional significance of side chains in this region of Raf_{55-132} is obtained by considering the distribution of conserved residues. Twenty-eight amino acid residues in Raf_{55-132} are conserved among a variety of species. Nine of these have buried side chains (colored dark blue in Figure 5c) and probably are conserved in order to maintain the fold. The remainder have exposed side chains (colored yellow and red in Figure 5c) and are distributed predominantly on one face of the protein. Comparison of panels a and c of Figure 5 reveals that the surface with the large cluster of conserved, exposed side chains is the same surface that interacts with Ras.

The binding site is not a uniform surface and possesses both indentations and protrusions. The major indentation is a cleft between the hairpin and the helix. This cleft is bridged by the side chain of Arg^{89}, which is directed toward the carbonyl group of Arg^{67} in the hairpin. Converting Arg^{89} to leucine substantially reduces the binding affinity of Raf toward Ras (Fabian et al., 1994; Lu et al., 1994). It is not known whether in the presence of Ras this side chain extends out to make a direct contact, in which case conversion to leucine could remove its ability to interact favorably, or if the mutation to leucine reduces binding activity by disrupting a particular spatial arrangement of the α-helix and the β-hairpin in Raf.

Binding site residues 66−69 are part of a β-strand (residues 66−72) that lacks a second partner in the sheet and whose backbone atoms could form intermolecular hydrogen bonds in a complex. It has been shown by systematic mutagenesis that the surface of Ras that binds to Raf consists of two principal elements: (1) the "effector loop", which is composed of residues 32−36 from loop 2 and residues 37−40 from β-strand 2, and (2) a segment of β-strand 3 comprised of residues 56−59, which is adjacent to the effector loop (Zhang et al., 1993; Chuang et al., 1994; Shirouzu et al., 1994; Herrmann et al., 1995). These regions contain hydrophobic residues and two negatively charged residues, Asp^{38} and Asp^{57}, which have been shown to be critical for binding. A possible Raf−Ras binding mode could be the antiparallel association of edge β-strands from each protein. Such an association could bury many of the Ras residues implicated in binding by mutagenesis studies. This binding mode would be analogous to that observed in a complex of protein G with an IgG Fab fragment (Derrick & Wigley, 1992; Lian et al., 1994), wherein edge β-strands from each protein make intermolecular hydrogen bonds in an

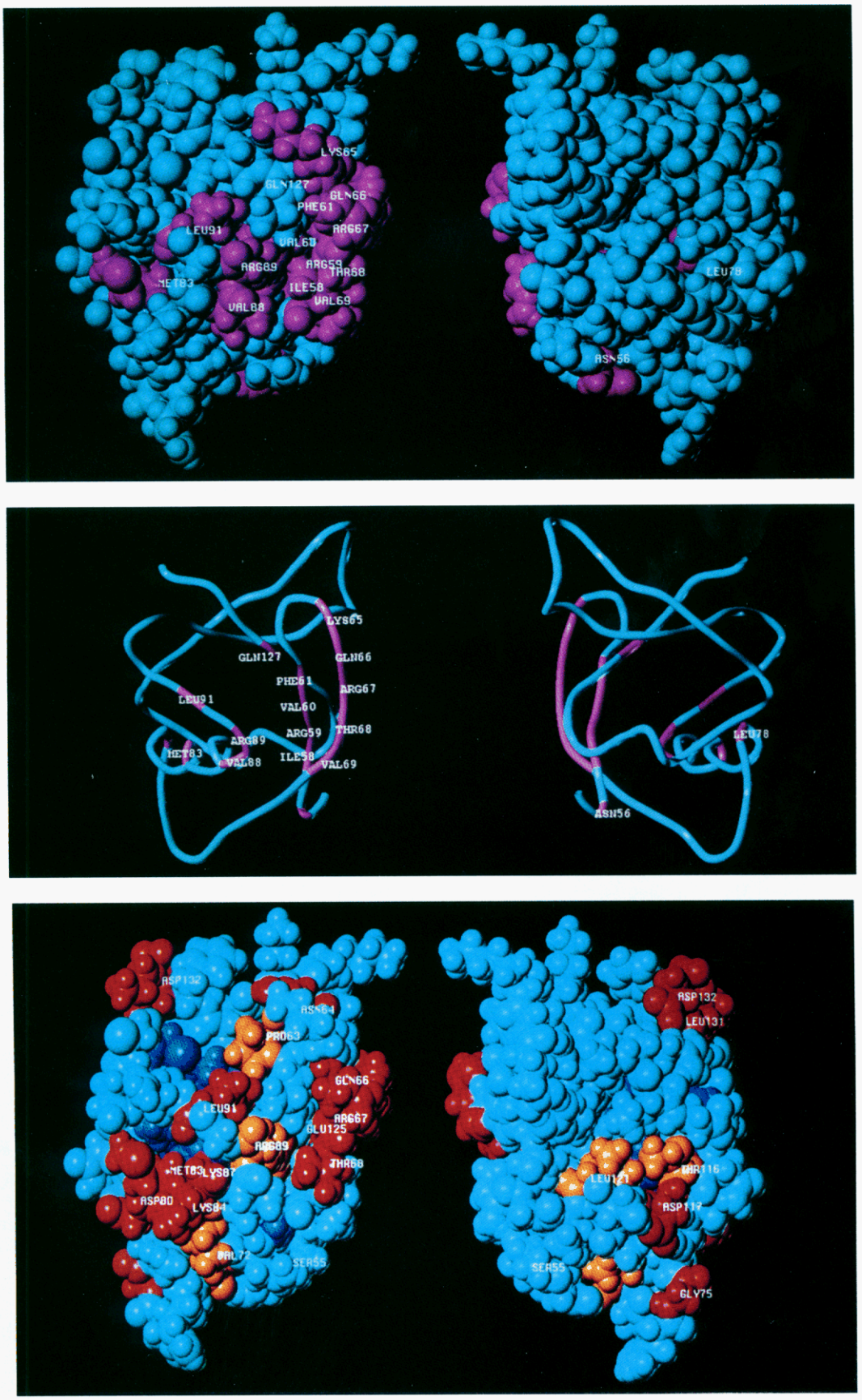

FIGURE 5: Space-filling and backbone−tube depictions of Raf_{55-132} identifying residues perturbed by the binding of Ras−GMPPNP (a, top, and b, center) and conserved residues (c, bottom). The lowest energy structure from among the 30 calculated structures is shown. The depictions are presented as pairs which differ by 180° around the z axis, in order to show both faces of the protein. (a and b) Residues which were most perturbed (see text) by addition of Ras−GMPPNP are colored magenta. (c) Conserved residues are colored according to the orientation of their side chains: buried (dark blue); positioned against the body of the protein (yellow); directed outward (red).

antiparallel pattern and hydrophobic side chains from both proteins are buried. The Fab-binding region of protein G is comparable to the Ras-binding region of Raf_{55-132} in that it is localized to the N-terminal β-hairpin and the C-terminus

of the α-helix.

In summary, the finding that Raf_{55-132} is a self-contained structural domain and the observation that it resembles a known, highly stable fold strongly suggest that this structure is maintained within the context of the intact 74 kDa Raf protein. We are testing this suggestion by studying longer fragments of Raf that include the 55−132 region. The Ras-binding domain is a rare example of an independently structured protein module identified initially on the basis of function (Vojtek et al., 1993), rather than by sequence homology. The surface of Raf_{55-132} that interacts with Ras has been identified as a patch of residues with exposed side chains localized within the β-hairpin and the C-terminal end of the α-helix. This information is consistent with the reduced activity of a Raf R89L mutant and should be useful for guiding and interpreting more extensive mutagenesis studies.

ACKNOWLEDGMENT

We thank J. Birktoft, B. Graves, and A. Swain for helpful discussions and advice and our colleagues at Roche Basle for assistance with the MOLSCRIPT figure.

REFERENCES

Achari, A., Hale, S. P., Howard, A. J., Clore, G. M., Gronenborn, A. M., Hardman, K. D., & Whitlow, M. (1992) *Biochemistry 31,* 10449−10457.

Barbacid, M. (1987) *Annu. Rev. Biochem. 56,* 779−827.

Bax, A., Clore, G. M., & Gronenborn, A. M. (1990) *J. Magn. Reson. 88,* 425−431.

Brooks, B. R., Bruccoleri, R. E., Olafson, B. D., States, D. J., Swaminathan, S., & Karplus, M. (1987) *J. Comput. Chem. 4,* 187−217.

Brunger, A. T., Milburn, M. V., Tong, L., deVos, A. M., Jancarik, J., Yamaizumi, Z., Nishimura, S., Ohtsuka, E., & Kim, S. H. (1990) *Proc. Natl. Acad. Sci. U.S.A. 87,* 4849−4853.

Chuang, E., Barnard, D., Hettich, L., Zhang, X. F., Avruch, J., & Marshall, M. S. (1994) *Mol. Cell. Biol. 14,* 5318−5325.

Davis, A. L., Keeler, J., Laue, E. D., & Moskau, D. (1992) *J. Magn. Reson. 98,* 207−216.

Derrick, J. P., & Wigley, D. B. (1992) *Nature 359,* 752−754.

deVos, A. M., Tong, L., Milburn, M. V., Matias, P. M., Jancarik, J., Noguchi, S., Nishimura, S., Miura, K., Ohtsuka, E., & Kim, S. H. (1988) *Science 239,* 888−893.

DiStefano, D. L., & Wand, A. J. (1987) *Biochemistry 26,* 7272−7281.

Emerson, S. D., Waugh, D. S., Scheffler, J. E., Tsao, K.-L., Prinzo, K. M., & Fry, D. C. (1994) *Biochemistry 33,* 7745−7752.

Fabian, J. R., Vojtek, A. B., Cooper, J. A., & Morrison, D. K. (1994) *Proc. Nat. Acad. Sci. U.S.A. 91,* 5982−5986.

Fry, D. C., Madison, V. S., Greeley, D. N., Felix, A. M., Heimer, E. P., Frohman, L., Campbell, R. M., Mowles, T. F., Toome, V., & Wegrzynski, B. B. (1992) *Biopolymers 32,* 649−666.

Gronenborn, A. M., Filpula, D. R., Essig, N. Z., Achari, A., Whitlow, M., Wingfield, P. T., & Clore, G. M. (1991) *Science 253,* 657−661.

Heidecker, G., Kolch, N., Morrison, D. K., & Rapp, U. R. (1992) *Adv. Cancer Res. 58,* 53−73.

Herrmann, C., Martin, G. A., & Wittinghofer, A. (1995) *J. Biol. Chem. 270,* 2901−2905.

Hyberts, S. G., Goldberg, M. S., Havel, T., & Wagner, G. (1992) *Protein Sci. 1,* 736−751.

Ikura, M., Kay, L. E., Tschudin, R., & Bax, A. (1990) *J. Magn. Reson. 86,* 204−209.

John, J., Sohmen, R., Feuerstein, J., Linke, R., Wittinghofer, A., & Goody, R. S. (1990) *Biochemistry 29,* 6058−6065.

Kay, L. E., Keifer, P., & Saarinen, T. (1992) *J. Am. Chem. Soc. 114,* 10663−10665.

Kraulis, P. J. (1991) *J. Appl. Crystallogr. 24,* 946−950.

Kraulis, P. J., Domaille, P. J., Campbell-Burk, S. L., Van Aken, T., & Laue, E. D. (1994) *Biochemistry 33,* 3515−3531.

Lian, L. Y., Derrick, J. P., Sutcliffe, M. J., Yang, J. C., & Roberts, G. C. K. (1992) *J. Mol. Biol. 228,* 1219−1234.

Lian, L. Y., Barsukov, I. L., Derrick, J. P., & Roberts, G. C. K. (1994) *Nature Struct. Biol. 1,* 355−357.

Lu, X., Melnick, M. B., Hsu, J.-C., & Perrimon, N. (1994) *EMBO J. 13,* 2592−2599.

Marion, D., Ikura, M., Tschudin, R., & Bax, A. (1989) *J. Magn. Reson. 85,* 393−399.

Milburn, M. V., Tong, L., deVos, A. M., Brunger, A., Yamaizumi, Z., Nishimura, S., & Kim, S. H. (1990) *Science 247,* 939−945.

Miller, A. F., Papastavros, M. Z., & Redfield, A. G. (1992) *Biochemistry 31,* 10208−10216.

Moodie, S. A., Willumsen, B. M., Weber, M. J., & Wolfman, A. (1993) *Science 260,* 1658−1661.

Pai, E. F., Kabsch, W., Krengel, U., Holmes, K. C., John, J., & Wittinghofer, A. (1989) *Nature 341,* 209−214.

Pai, E. F., Krengel, U., Petsko, G. A., Goody, R. S., Kabsch, W., & Wittinghofer, A. (1990) *EMBO J. 9,* 2351−2359.

Presta, L. G., & Rose, G. D. (1988) *Science 240,* 1632−1641.

Rodriguez-Viciana, P., Warne, P. H., Dhand, R., Vanhaesebroeck, B., Gout, I., Fry, M. J., Waterfield, M. D., & Downward, J. (1994) *Nature 370,* 527−532.

Scheffler, J. E., Waugh, D. S., Bekesi, E., Kiefer, S. E., LoSardo, J. E., Neri, A., Prinzo, K. M., Tsao, K.-L., Wegrzynski, B., Emerson, S. D., & Fry, D. C. (1994) *J. Biol. Chem. 269,* 22340−22346.

Shirouzu, M., Koide, H., Fujita-Yoshigaki, J., Oshiro, H., Toyama, Y., Yamasaki, K., Fuhrman, S. A., Villafranca, E., Kaziro, Y., & Yokoyama, S. (1994) *Oncogene 9,* 2153−2157.

Tong, L., deVos, A. M., Milburn, M. V., & Kim, S. H. (1991) *J. Mol. Biol. 217,* 503−516.

Trahey, M., & McCormick, F. (1987) *Science 238,* 542−545.

Trahey, M., Miller, R. J., Cole, G. E., Innis, R. M., Patterson, H., Marshall, C. J., Hall, A., & McCormick, F. (1987) *Mol. Cell. Biol. 7,* 541−544.

Van Aelst, L., Barr, M., Marcus, S., Polverino, A., & Wigler, M. (1993) *Proc. Natl. Acad. Sci. U.S.A. 90,* 6213−6217.

Vijay-Kumar, S., Bugg, C. E., & Cook, W. J. (1987) *J. Mol. Biol. 194,* 531−544.

Vojtek, A. B., Hollenberg, S. M., & Cooper, J. A. (1993) *Cell 74,* 205−214.

Warne, P. H., Viciana, P. R., & Downward, J. (1993) *Nature 364,* 352−355.

Weber, P. L., Brown, S. C., & Mueller, L. (1987) *Biochemistry 26,* 7282−7290.

Zhang, X., Settleman, J., Kyriakis, J. M., Takeuchi-Suzuki, E., Elledge, S. J., Marshall, M. S., Bruder, J. T., Rapp, U. R., & Avruch, J. (1993) *Nature 364,* 308−313.

BI950471B